MOLECULAR PHYSICS, 1996, VOL. 87, NO. 2, 299–318 100444

Rotationally resolved magnetic vibrational circular dichroism

Experimental spectra and theoretical simulation for diamagnetic molecules

By PETR BOUR†, CHEOK N. TAM, BAOLIANG WANG and TIMOTHY A. KEIDERLING

Department of Chemistry, University of Illinois at Chicago, 845 W. Taylor, Chicago, IL 60607, USA

(Received 24 July 1995; accepted 29 August 1995)

The rotationally resolved magnetic vibrational circular dichroism (RR MVCD) spectra of the diamagnetic molecules DCl and NH_3 are analysed on the basis of theoretical simulation. Basic theoretical equations are derived for the RR MVCD dispersed intensity pattern from the conventional rovibrational energy level expression. This provides a convenient method for interpretation of MVCD spectra in terms of fundamental spectroscopic parameters. Good agreement was obtained between the simulated and the experimental data measured for DCl and NH_3. Minor deviations from the theory occur in the dipole strength distribution for DCl, but this is corrected by measuring the A_1/D_0 ratio, from which the molecular g value can be determined for resolved transitions. Although magnetic properties of DCl and NH_3 are known, this study demonstrates the ability of MVCD to provide an alternate method of determining molecular g-values as compared to classical microwave studies of the Zeeman effect. The data further show that experimentally observed RR MVCD spectra are fully explained using the conventional theory for rovibrational transitions under Zeeman perturbation. Variations of magnetic parameters of the ground and excited vibrational states of these molecules cause characteristic changes of the MVCD band intensity patterns. These variations are used to evaluate approximations made in previous moment analyses of RR MVCD spectra and to delimit the sensitivity of the RR MVCD technique to differences in ground and excited state g-values.

1. Introduction

Magnetic vibrational circular dichroism (MVCD) was first observed in 1981 {1}. Since then MVCD has been the focus of both experimental and theoretical studies in our laboratory. MVCD of several relatively small symmetric and spherical top molecules and a large number of porphyrin derivatives have been measured in the condensed phase {2–10}. Meanwhile, a theoretical model based on the vibronic coupling between ground and excited electronic states {11–13} has been proposed and used for the analysis of the MVCD of several of these molecules. Recently, our studies have been extended to measure the molecular rotational and vibrational Zeeman g values for rotationally resolved (RR) MVCD spectra of a few small molecules in the gas phase. MVCD spectra sense molecular Zeeman effects {14–17} which in general are quite small in terms of molecular energy perturbation but have proven to be easily measurable with this technique.

† Permanent address: Institute of Organic Chemistry and Biochemistry, Academy of Sciences of the Czech Republic, Flemingovo nam. 2, 16610, Praha 6, Czech Republic.

Good agreement, within the limits of the technique, was found between the RR MVCD derived rotational g values for carbon monoxide {14}, hydrogen chloride and deuterium chloride {15} and more precise g values derived earlier from microwave or molecular beam magnetic resonance measurements {18–22}. These experiments on diatomics effectively provided an experimental calibration of the technique to demonstrate that RR MVCD can be used to evaluate the molecular Zeeman effect. The analysis of the MVCD of polyatomics, for example NH_3 and CH_4, to determine molecular g values necessarily involved a number of approximations in order to use the same sort of methods shown applicable for diatomics. Going beyond such approximations is the topic of this paper.

In our previous RR MVCD reports, the relationship between the molecular Zeeman g value and the MVCD A_1/D_0 parameter was derived {14–16} by using the approximation that g values for the vibrational excited and ground states are the same, i.e. $g_{v=1} = g_{v=0}$. This approximation was justified in the cases of CO, HCl and DCl for which there is, in fact, no significant difference between $g_{v=1}$ and $g_{v=0}$ {14, 15}. Our analyses of those data indicate that the prime variation in experimental A_1/D_0 values for different v and J states was due to random error. Determination of A_1/D_0 was based on a line by line moment analysis of the observed MVCD and absorption spectra {14, 15}. In those calibration experiments, the variation in the ratios of the moments was used to evaluate the overall error of the method.

Traditionally, high resolution spectra of polyatomics have been analysed by generation of the rovibrational structure and intensities using a model Hamiltonian and comparison of a simulated spectrum based on a reasonable spectral width, as compared to that of the experiment. Using a suitable Hamiltonian and adaption of selection rules to represent the measured differential spectrum, one can also simulate the MVCD spectra. For some small molecules, sufficient experimental data and theoretical results exist for MVCD simulation. But for many there is insufficient data, particularly for vibrational excited states. By varying the simulation parameters and comparison to experimental MVCD spectra, the effect of these unknown parameters on the spectra can be evaluated. Furthermore, the effect of any approximations made in analysing the MVCD spectra can be tested using the simulated spectra both qualitatively and quantitatively, since the theoretical parameters are known. In this paper, simulations of the MVCD for two example diamagnetic molecules are reported, one diatomic and one symmetric top, DCl and NH_3. The simulated spectra will then be compared with the available experimental data.

2. Calculational method

2.1. Spectra of diatomics

The rovibrational energy levels of diatomic diamagnetic molecules are well known {23, 24}. These energies can be expressed by the expansion:

$$\varepsilon_{vJ} = \varepsilon_v + hcB_e J(J+1) + hc\alpha_e J(J+1)(v+1/2) - hcD_v J^2(J+1)^2 \qquad (1)$$

where ε_v is the experimentally determined vibrational frequency, B_e is the equilibrium rotational constant, α_e is the rotation–vibration interaction constant and D_v is the centrifugal distortion constant for the vibrational level v. B_e and α_e are normally

Table 1. Input parameters used for the RR MVCD spectra simulation for deuterium chloride.

Parameter	$D^{35}Cl$
$\frac{\varepsilon_v}{hc}/cm^{-1}$ [a]	2091·0778
B_e/cm^{-1}	5·44847
$D_0/10^{-6}\,c^{-1}$	139·96
g value, $v = 0$	0·235
g value, $v = 1$	0·235
T/K	298
α/cm^{-1}	0·11181
c_1 [b]	0
c_2 [b]	0
$B/tesla$ [c]	10

[a] $1\ cm^{-1} = 2{\cdot}998 \times 10^{10}$ Hz.

[b] No experimental data available in the literature.

[c] 1 tesla = 10000 Gauss.

expressed in units of cm^{-1}, which leads us to explicitly include h, Planck's constant, and c, the velocity of light. Under the influence of an external field, the degenerate rotational states split into $2J+1$ levels which are characterized by M values, the projection of the molecular angular momentum on the magnetic field direction. Using the rotational g values from the literature {25}, the rovibrational sublevel energies can be calculated by adding a Zeeman energy term,

$$\varepsilon_{vJM} = \varepsilon_{vJ} - g_J \mu_N \mathscr{B}_z M \tag{2}$$

where μ_N is the nuclear magneton and $\mathscr{B}_z$ is the magnetic field strength along the light propagation vector.

The fundamental formulae developed for the theory of electronic magnetic circular dichroism (MCD) by Stephens {26} can be applied here. The basic differences relate to the wavefunctions used and the absolute selection rules for rotationally resolved spectra, as given by the conservation of angular momentum, whereby the quantum number M can change to $M+1$ by an absorption of a left circularly polarized photon and to $M-1$ for absorption of a right circularly polarized photon. The dipole-moment matrix elements were evaluated by the means of the Wigner–Eckart theorem {27}, to calculate the RR MVCD intensities, as described in Appendix A. The line strengths of each transition, $|v = 0, J'', M''\rangle \rightarrow |v = 1, J', M'\rangle$, of frequency ω, for left (L) and right (R) circularly polarized light, were calculated according to the expression:

$$A_{L/R} = \kappa\omega\xi(2J+1)^{-1}|\langle J' - M'1 \pm 1 \,|\, J'' - M''\rangle|^2 C_{HWF}\mu^2 \exp(-\varepsilon_{0,J''}/kT) \tag{3}$$

where the Clebsch–Gordan coefficients, $\langle J' - M'1 \pm 1 \,|\, J'' - M''\rangle$, distinguish selection rules for L/R circularly polarized light; κ is a constant independent of the frequency; C_{HWF} is the Herman–Wallis factor {28}: $C_{HWF} = 1 + c_1 j + c_2 j^2$ with $j = -J''$ for the P-branch and $j = J''+1$ for the R branch; ξ is the Honl–London factor: $\xi = J''+1$ for R branch and $\xi = J''$ for P branch; $\varepsilon_{0,J''}$ is the energy of the initial state of the rovibrational

absorption transition relative to the ground state; k is the Boltzman constant; T is the temperature; and μ is the absolute value of the vibrational dipole transition moment. The intensity of the absorption and MVCD spectra can be calculated as $(A_L + A_R)/2$ and $(A_L - A_R)$, respectively. The factor of two is needed for simulation of the absorbance measurement because the beam polarization oscillates between L and R, and the absorbance experiment averages over this oscillation, and the $\Delta A = A_L - A_R$ conforms to the standard chemistry convention.

Absorption and MVCD spectra of the diatomics were generated from the calculated frequencies and intensities at 298 K by a set of computer programs written in house. The input spectral parameters are listed in table 1. Calculation of the RR MVCD intensities as well as the generation of the simulated spectra in the Spectracalc format {29} were done on an IBM-compatible PC/386 computer within a few minutes. The bandshapes used in these simulated spectra were linear combinations of Gaussian and Lorentzian bandshapes which were taken from the best fit of such combined bandshapes to our experimental absorption spectra. We used the absorption spectra simulation program Contour {30} to check that our program properly simulated the absorption spectra pattern. Owing to the relatively low resolution used, the experimental absorption spectra profiles are not affected by the magnetic field.

2.2. Spectra of symmetric top molecules

In the case of the NH_3 molecule, symmetric top rotational wavefunctions are used along with the standard expression for the energy levels:

$$\varepsilon^{\pm}_{vJKM} = \varepsilon^{\pm}_{v} + hc\{B^{\pm}_{v} J(J+1) + (C^{\pm}_{v} - B^{\pm}_{v}) K^2 - D^{\pm}_{vJK} J(J+1) K^2 - D^{\pm}_{vJ} J^2(J+1)^2 - D^{\pm}_{vK} K^4\} - g^{\pm}_{vJK} \mu_N M \mathcal{B}_z \quad (4)$$

where the indices + and − denote the symmetric and antisymmetric vibrational states, respectively, with respect to the double-well potential corresponding to motion along the molecular inversion coordinate. K is the projection of the angular momentum on the molecular axis. For the rotational constants the common notation is used {24}. The dependence of the rotational g value on the J and K quantum numbers is given by

$$g^{\pm}_{vJK} = g^{\pm}_{v,xx} + (g^{\pm}_{v,zz} - g^{\pm}_{v,xx}) \frac{K^2}{J(J+1)} \quad (5)$$

where $g^{\pm}_{v,zz}$ and $g^{\pm}_{v,xx}$ are components of the g tensor written in the molecular coordinate system.

The line strengths for each $|v''J''K''M''\rangle \rightarrow |v'J'K'M'\rangle$ transition can be calculated as:

$$A_{L/R} = \kappa\omega \frac{2J'+1}{2J''+1} |\langle 10 J'K' | J''K''\rangle|^2 |\langle J' - M' 1 \pm 1 | J'' - M''\rangle|^2 \times \mu^2 g_K g_I \exp(-\varepsilon_{0,J'',K''}/kT) \quad (6)$$

where ω is the frequency of the transition, g_K is the degeneracy of the K level, g_I is a statistical factor which is determined by the symmetry of the nuclear wavefunctions {23, 24}. Other symbols are same as defined in equation (3). Again, the Clebsch–Gordan

Table 2. Input parameters used for the simulation of the RR MVCD spectrum of ammonia.

Parameter	Sym (+) state	Asym (−) state	Units
B_0	9·946642	9·941589	cm^{-1}
B_1	10·070178	9·890022	cm^{-1}
C_0	6·228362	6·230362	cm^{-1}
C_1	6·089170	6·160685	cm^{-1}
D_{0J}	0·84952	0·83273	$10^{-3}\,cm^{-1}$
D_{1J}	1·13078	0·69700	$10^{-3}\,cm^{-1}$
D_{0JK}	−1·57829	−1·53196	$10^{-3}\,cm^{-1}$
D_{1JK}	−2·42260	−1·23452	$10^{-3}\,cm^{-1}$
D_{0K}	1·01069	0·97894	$10^{-3}\,cm^{-1}$
D_{1K}	1·61718	0·81096	$10^{-3}\,cm^{-1}$
g_{0xx}	0·5657	0·5657	
g_{1xx}	0·5901	0·5791	
g_{0zz}	0·5027	0·5027	
g_{1zz}	0·5140	0·5064	
$\omega(0-\rightarrow 1+)$	931·58		cm^{-1}
$\omega(0+\rightarrow 1-)$	968·08		cm^{-1}
$\omega(0+\rightarrow 0-)$	0·66		cm^{-1}
Temperature	298		K
Magnetic field	1		Tesla

coefficients determine the selection rules $\Delta M = \pm 1$. Additionally, for the umbrella mode, only the transitions with $K' = K''$ are allowed. For the vibrational states the selection rules allow the $0^- \rightarrow 1^+$ and $0^+ \rightarrow 1^-$ transitions.

Absorption and RR MVCD spectra were simulated in the same manner as described for the diatomics using the input parameters listed in table 2 {25, 31}.

2.3. Analysis of simulated spectra

To provide a basis of comparison to our previous experimental studies, all simulated spectra were analysed using moment analysis techniques {26, 32}. MVCD A terms were characterized by the A_1/D_0 parameter, determined as:

$$\frac{A_1}{D_0} = \frac{\langle \Delta A \rangle_1}{\beta \mathcal{B}_z \langle A \rangle_0} \tag{7}$$

where β is the Bohr magneton, and the zeroth moment of the absorbance and the first moment of the MVCD are defined as

$$\langle A \rangle_0 = \int (A/\nu)\, d\nu \quad \text{and} \quad \langle \Delta A \rangle_1 = \int (\Delta A/\nu)(\nu - \nu_0)\, d\nu,$$

respectively. Thus effective g values for these theoretical spectra were calculated as

$$g_e = -\frac{1}{2}\frac{\beta}{\mu_N}\frac{A_1}{D_0}. \tag{8}$$

These effective g values were then compared with the input true rotational g values to test the validity of the moment analysis scheme. More importantly, determination of

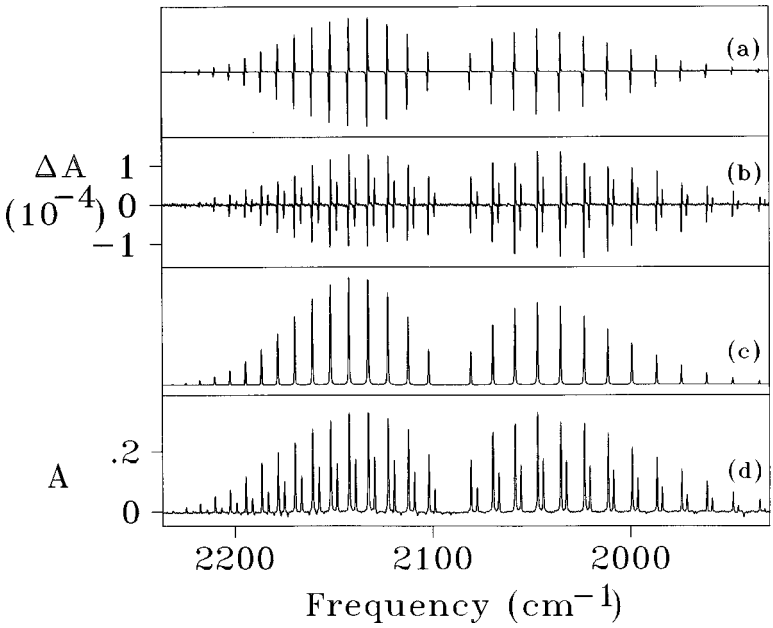

Figure 1. (a) The simulated RR MVCD spectrum of $D^{35}Cl$ at 1 tesla, (b) the experimental spectrum of naturally occurring DCl at a resolution of 0·5 cm^{-1}, normalized to 1 tesla; (c) the simulated absorption spectrum of $D^{35}Cl$; and (d) the experimental spectrum of naturally occurring DCl at a resolution of 0·5 cm^{-1}. Experimental data were obtained previously {15}.

g_e from both simulation and experimental spectra provides a quantitative check on the accuracy of the theoretical parameters postulated via this simulation process.

In the case for which the g value in the $v = 1$ state is not equal to the g value for $v = 0$, we simply input two different g values into the simulation of the corresponding spectra using the method described above. Moment analyses were then carried out to determine the A_1/D_0 values and subsequently the effective g values, g_e, were determined using equation (8). The relationship found between $g_{v=0}$, $g_{v=1}$ and g_e and qualitative diagnostics that can be developed for MVCD intensity patterns will be discussed in the following sections.

3. Results

3.1. Spectral simulation

The simulated RR MVCD spectra of $D^{35}Cl$ are shown in figure 1(a) and compared to the 0·5 cm^{-1} resolution experimental data for natural abundance DCl given in figure 1(b) {15}. The corresponding simulated and experimental absorption spectra are in figure 1(c) and 1(d) respectively. In general, excellent agreement between theoretical and experimental MVCD spectra is achieved except for the relative dipole intensities of the R branch and P branches. Since the same relative intensity pattern is seen in the absorption simulation, this disparity is due to the dipole intensity term whose effect is exacerbated in the respective MVCD due to convolution with the A term derivative lineshape. These simulated spectra use the same rotational g value in the $v = 1$ vibrational state as in the $v = 0$ state.

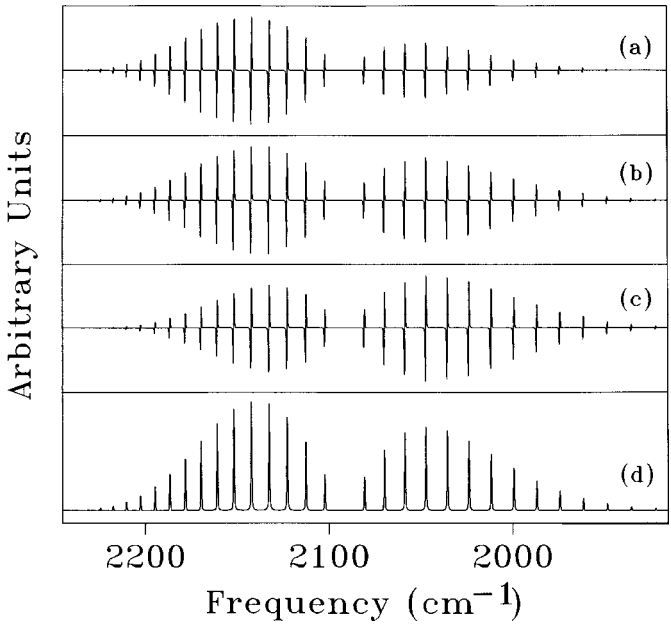

Figure 2. The simulated RR MVCD spectrum of D^{35}Cl at 1 tesla with (a) $g_{v=1}/g_{v=0}$ = 1·1;) (bim

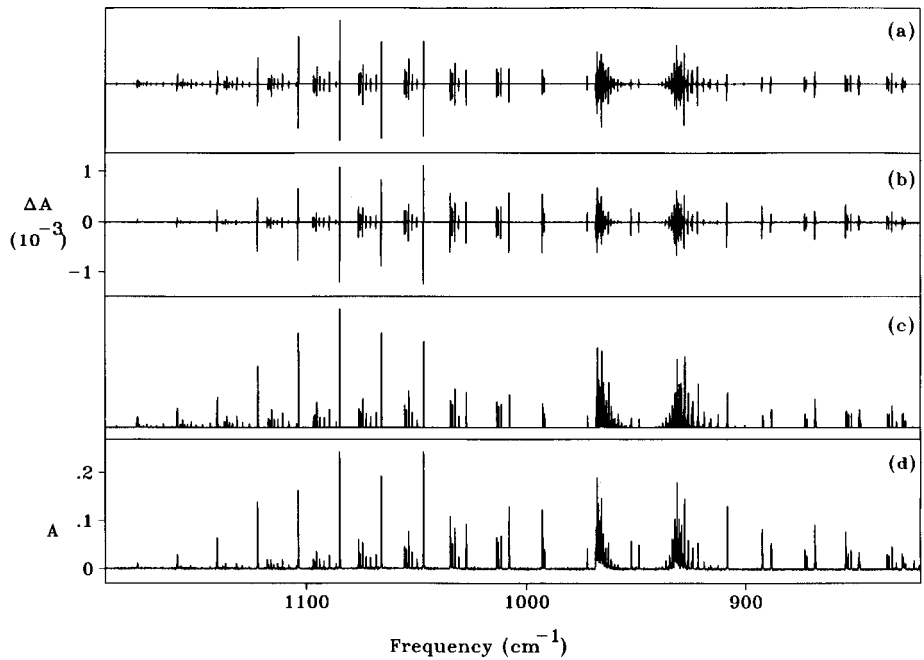

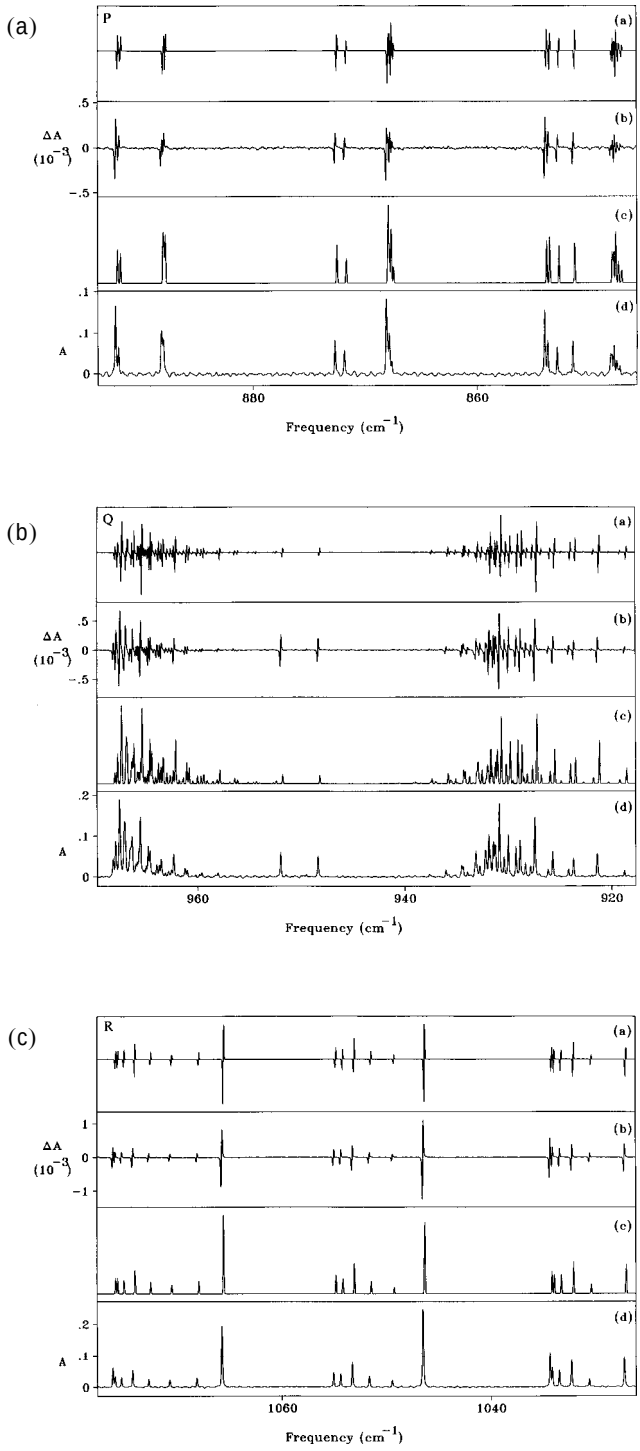

Figure 4. Expanded representation of the experimental and simulated MVCD and absorption spectra of: (a) part of the P branches of NH_3 at 1 tesla; (b) the Q branch region (symmetric and asymmetric); (c) part of the R branch region details of each spectrum (a)–(d) as in figure 3.

To investigate the consequences of $g_{v=1} \neq g_{v=0}$ on a system of minimal complexity, MVCD spectra of $D^{35}Cl$ were simulated with various $g_{v=1}/g_{v=0}$ ratios as shown in figure 2. Changing $g_{v=1}$ with respect to $g_{v=0}$ modifies the relative intensities of the P and R branches. For $g_{v=1}/g_{v=0} = 1{\cdot}1$, the intensity of the R branch increases while that of P branch diminishes (figure 2(a)). The opposite trend was observed for the $g_{v=1}/g_{v=0} = 0{\cdot}9$ case (figure 2(c)). At this resolution ($0{\cdot}5\ cm^{-1}$), the absorbance spectrum, figure 2(d), is unaffected by the g values. As discussed in the next section, moment analyses provide an alternative means of evaluating the effect of g value variation.

The rovibrational spectrum of the ν_2 mode of NH_3 is relatively complex due, in part, to there being two sets of overlapping P, Q and R branches and, in part, due to the K dependence of the energy levels {16}. Therefore, we remeasured the absorption and RR MVCD spectra of NH_3 at a higher resolution of $0{\cdot}1\ cm^{-1}$ using a BIORAD Digilab FTS-60A spectrometer coupled to our previously described MVCD optical bench {33–35}. This upgrade will be detailed separately {36–38} and experimental details relevant to the example here are in the figure captions. Figure 3 summarizes the simulated MVCD and absorption spectra for the entire observable ν_2 mode of NH_3, while figures 4(a), 4(b) and 4(c) show expanded sections of the simulated and experimental spectra of the P, Q and R branches, respectively, to illustrate the simulation of individual lineshapes. Excellent qualitative agreement between the simulated and experimental MVCD spectra is again achieved in spite of the modest S/N in the high J region of the P and R branches. The relative simulated absorbance intensities again are in some disagreement with experiment which affects the simulated MVCD intensity distribution. In all cases, comparison of the A_1/D_0 ratio for experimental and simulated spectra corrects this difficulty. Although the peaks in the Q branches are closely overlapped and overlap P branch transitions for low J values, the similarity and consistency seen between the simulated and the experimental MVCD spectra of the Q branches assure us that the experimental MVCD spectra found for these Q branches are real and not due to noise or artifacts, as was thought possible in our original analysis {16}. Owing to our current resolution limit of $0{\cdot}1\ cm^{-1}$, many K components, particularly in the R branches for the symmetric bands, are not resolved (note that there is no intrinsic limit in resolution associated with the MVCD technique). However, the simulation is able to reproduce the observed spectra of the overlapping K components reasonably well using a consistent linewidth of $0{\cdot}1\ cm^{-1}$ and just a Gaussian lineshape.

3.2. Analyses of simulated MVCD spectra

Firstly we tested the precision of the moment analysis on the simulated spectrum. For the $g_{v=1} = g_{v=0}$ case the $D^{35}Cl$ parameters from table 1 were used. The effective g value, g_e, obtained from the moment analysis of the simulated spectra was 0·234. The error in the curve fitting process used to interpret our spectra is thus less than 0·1 %, which demonstrates that our method of moment analysis is applicable for determining the g value. The improvement in precision compared to our earlier calibration tests on real experimental data implies that the error found in experimental MVCD g values can be attributed to S/N limitations rather than to the analysis method.

For the $D^{35}Cl$ $g_{v=1}/g_{v=0} = 0{\cdot}9$ simulation (figure 2(c)), the A_1/D_0 ratio and the apparent g value, g_e, systematically vary with J''. The Wigner–Eckart theorem leads to

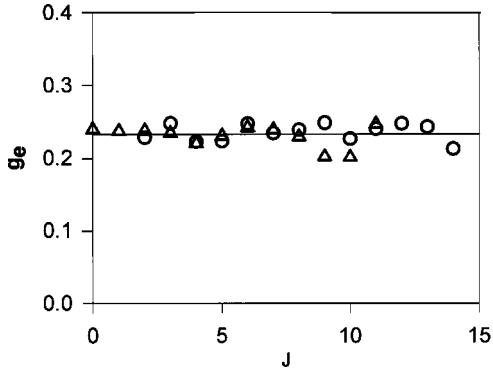

Figure 5. The plots of g_e values determined by moment analysis of the experimental absorption and RR MVCD spectra of DCl against J for P branch (circles) and R branch (triangles), where J = J″+1 and J = J″ for the P and R branches, respectively. The solid line indicates theoretical values with g_J = 0·235 for all J″ values. If Δg (equation (9)) were measurably non-zero, the best lines through the triangles and circles would diverge at high J-values.

the following dependencies of g_e on the rotational J″ number when the g_J values for the ground and excited states are different:

$$g_e = g_{v=1} - (J''+1)\frac{\Delta g}{2}, \quad \text{(P branch, } J' = J''-1) \tag{9a}$$

$$g_e = g_{v=1} - \frac{\Delta g}{2}, \quad \text{(Q branch, } J' = J'') \tag{9b}$$

$$g_e = g_{v=1} + J''\frac{\Delta g}{2}, \quad \text{(R branch, } J' = J''+1) \tag{9c}$$

where $\Delta g = g_{v=1} - g_{v=0}$. The derivation of equation (9) is given in Appendix B. As can be seen, when $g_{v=1} > g_{v=0}$, the g_e values for the P branch decrease and those for the R branch will grow as J″ increases, as is illustrated in the simulated spectra shown in figure 2. Moreover, the g_e value should be linearly dependent on J″ so that the slope of a plot of g_e against J″ would give $\Delta g/2$ and the y intercept $g_{v=1}$.

This analysis has been applied to the experimental DCl MVCD data in figure 1 by plotting the results of our earlier moment analyses. These distributions of g_e against J″ are effectively flat with an intercept of 0·235 (figure 5). A pooled t-test has been applied to the DCl R branch data and used to show that a non-zero slope would be statistically insignificant. Similar conclusions have been made when the same test was applied to experimental HCl and CO MVCD data which formed the other 'calibration' tests we have published {14, 15}. Although the MVCD intensity distribution alone might seem to suggest that $g_{v=1}/g_{v=0} < 1$, it is important to note that the simulation underestimates the dipole strength of the P branch. Plotting the A_1/D_0 values as a function of J provides a more critical means of sensing variance in excited and ground state g values. Thus it is critical to reduce the spectra to such a normalized representation as A_1/D_0 in order to evaluate relative g values for various transitions.

Since the ammonia spectra are complex, some of the bands are not well resolved, especially the K components of the rotational transitions in the symmetric band. This applies to the simulation as well since we used a constant linewidth (0·1 cm^{-1} FWHH)

Table 3. Summary of the moment analysis of the simulated absorption and RR MVCD spectra for NH_3 ν_2 symmetric transitions.

Transition[a]	ν_0[b] cm^{-1}	A_1/D_0[c] ($\times 10^4$)	g_e^{exp}[d]	g_e^{sim}[e]
sP(1, 0)	948·22	− 7·2307	0·664	0·586
sP(2, 1)	928·22	− 6·0850	0·559	0·561
sP(3, K)	908·17	− 9·3405	0·858	0·555
*sP(4, K)	888·07	− 9·0312	0·829	0·551
*sP(5, K)	867·99	− 6·6336	0·609	0·544
sR(1, K)	1007·54	− 7·0854	0·650	0·585
sR(2, K)	1027·04	− 7·6113	0·699	0·589
sR(3, K)	1046·40	− 8·0507	0·739	0·595
sR(4, K)	1065·58	− 8·2277	0·755	0·599
sR(5, K)	1084·60	− 8·5904	0·789	0·605
sR(6, K)	1103·46	− 8·3330	0·765	0·606
sR(7, K)	1122·15	− 9·3192	0·856	0·616
sR(8, K)	1140·64	− 11·9145	1·094	0·618

[a] sR(J″, K″) is a commonly used notation for the rotation–vibration double-inversion transitions where a and s indicate the parity of the total eigenfunction of the ground state with respect to the inversion of all particles about the centre of mass.

[b] ν_0 is determined by setting $\langle A \rangle_1 = 0$ and thus may vary from accepted values due to inclusion of overlapped transitions.

[c] A_1/D_0 from the experimental spectra is evaluated according to equation (7).

[d] g values from the experimental spectra.

[e] g values from the simulated spectra.

* Less reliable results from overlapped bands.

for the calculated spectra which is close to experimental linewidths (obtained with a nominal 0·1 cm^{-1} resolution). The results of moment analysis of the simulated absorption and MVCD spectra of the ν_2 mode of ammonia are summarized in tables 3 and 4 including results from moment analysis of overlapped bands.

For each $|v = 0, J''K''\rangle$ and $|v = 1, J'K'\rangle$ rovibrational state, $g_{v=0}^{J'',K''}$ and $g_{v=1}^{J'',K''}$ can be evaluated by equation (5) and then used to calculate the g_e^{sim} for each transition by substituting $g_{v=0}^{J'',K''}$ for $g_{v=0}$ and $g_{v=1}^{J'',K''}$ for $g_{v=1}$ in equation (9). These theoretical simulation g values can also be extracted from the simulated spectra by using moment analysis whereby we have shown the apparent g_e to be identical to the calculated g_e^{sim} to less than 0·1% error. This demonstrates again the reasonability of our moment analysis technique for extracting meaningful g values from the experimental MVCD spectra of polyatomics. The NH_3 g_e^{sim} shows a trend of a slight increase in magnitude with increasing J″ in the R branch and decrease in the P branch which comes about from Δg (equation (9)) being positive. This change is less than 5% over the range of J″ values for which we have obtained reasonable RR MVCD spectra (table 3 and 4) and thus is probably smaller than our detectable limits for g value change as restricted by the S/N limitations of the NH_3 0·1 cm^{-1} RR MVCD data available. The g_e^{sim} of these resolved K components for a given J″ of these R(J″, K″) transitions generally increases and decreases with K″ for the P and R branches, respectively, but this variation with K″ is even smaller than the J″ dependence and is thus not experimentally detectable in these data.

With regard to the experimental NH_3 RR MVCD, there are significant differences between g_e^{sim} and g_e^{exp} as shown in tables 3 and 4. The experimental g values found are

Table 4. Summary of the moment analysis of the simulated absorption and RR MVCD spectra for NH_3 ν_2 asymmetric transitions.

Transition[a]	ν_0[b] cm^{-1}	A_1/D_0[c] ($\times 10^4$)	g_e^{expd}	g_e^{sime}
*aP(2, 0)	892·14	− 7·0791	0·650	0·553
*aP(2, 1)	891·86	− 7·1709	0·658	0·557
aP(3, 1)	872·54	− 9·7414	0·894	0·543
aP(3, 2)	871·71	− 7·3491	0·675	0·550
*aP(4, 0)	853·80	− 7·1630	0·658	0·529
*aP(4, 1)	853·52	− 6·3999	0·588	0·531
aP(4, 2)	852·70	− 10·5377	0·967	0·536
aP(4, 3)	851·30	− 7·2698	0·667	0·544
aP(5, 1)	834·80	− 7·9760	0·732	0·518
aP(5, 2)	833·99	− 7·2174	0·663	0·522
aP(5, 3)	832·61	− 11·7636	1·080	0·529
aR(0, 0)	951·77	− 7·8195	0·718	0·590
aR(1, 1)	971·88	− 8·0370	0·738	0·599
*aR(2, 0)	992·70	− 5·7850	0·531	0·614
*aR(2, 1)	992·44	− 6·7131	0·616	0·612
aR(2, 2)	991·68	− 7·6396	0·701	0·606
aR(3, 1)	1013·18	− 7·5011	0·689	0·625
aR(3, 2)	1012·44	− 8·9039	0·817	0·620
aR(3, 3)	1011·20	− 7·7790	0·714	0·612
*aR(4, 0)	1034·25	− 6·3533	0·583	0·639
*aR(4, 1)	1034·02	− 6·8875	0·632	0·638
aR(4, 2)	1033·32	− 6·5698	0·603	0·634
aR(4, 3)	1032·13	− 7·3870	0·678	0·627
aR(4, 4)	1030·42	− 6·2780	0·576	0·618
aR(5, 1)	1054·92	− 5·4674	0·502	0·650
aR(5, 2)	1054·26	− 6·3600	0·584	0·647
aR(5, 3)	1053·13	− 8·7589	0·804	0·641
aR(5, 4)	1051·51	− 8·5563	0·786	0·634
aR(5, 5)	1049·34	− 8·3849	0·770	0·624
*aR(6, 0)	1076·04	− 7·6953	0·706	0·663
*aR(6, 1)	1075·83	− 10·0790	0·925	0·662
aR(6, 2)	1075·21	− 7·9050	0·726	0·660
aR(6, 3)	1074·16	− 8·1976	0·753	0·655
aR(6, 4)	1072·63	− 5·5702	0·511	0·648
aR(6, 5)	1070·60	− 7·1968	0·661	0·640
aR(6, 6)	1067·98	− 5·7535	0·528	0·630

[a] aR(J″, K″) is a commonly used notation for the rotation–vibration double-inversion transitions where a and s indicate the parity of the total eigenfunction of the ground state with respect to the inversion of all particle about the centre of mass.

[b,c,d,e,*] As in table 3.

generally higher than the simulated values, but the trends are hard to discern given that there is a substantial variance from one J″ to the next. This discrepancy can be attributed to intrinsic random error in the intensity measurement. Going to 0·1 cm^{-1} resolution increased the signal size by five times over our earlier published 0·5 cm^{-1} result, but the noise level also increased due to our constraints on the available scan time for these high resolution experiments. The overall trend appears to be that as J″ increases in both R branches (symmetric and asymmetric), the observed g_e increases as well. The opposite trend is probably observed for both P branches but less reliable

Table 5. The dependence of the molecular g value on NH_3 geometry.

α	g_{xx}	g_{zz}
110·8	0·588	0·509
111·8	0·583	0·511
112·8	0·579	0·513
Exp	0·5657	0·5027

data is available for these transitions. For both branches, the high J values have anomalously high g values which are thought to be derived from their low intensities and consequently low S/N. This trend with J qualitatively fits the expectation of equation (9) and that seen in our simulation since the $g_{v=0}^{J'',K''}$ values are smaller than the $g_{v=1}^{J'',K''}$ values for both the symmetric and asymmetric vibrational states.

3.3. The influence of centrifugal distortion on the g value

To estimate the possible influence of the centrifugal distortion on the values of the g factor of ammonia, an ab initio calculation was performed for three different geometries of the molecule, varying α, the angle between the N–H bond and the C_3 axis. At the MP2/6-31G** determined equilibrium geometry, $\alpha = 111{\cdot}8°$; calculations were done at that value as well as for $\alpha = 110{\cdot}8°$ and $112{\cdot}8°$. Calculation of the magnetic properties (diamagnetic susceptibility) was performed at the Hartree–Fock level, using the CADPAC {39} system of programs and its standard 6-31G extended basis set (6-31G + p + d + two sets of polarization functions). The one-degree variation in the H–N–H angle chosen for this test corresponds approximately to the change in geometry expected in varying J″ from J″ = 0 to J″ = 10, as can be estimated by the comparison of calculated and tabulated effective rotational constants, $B_{J''}$. This interval approximately covers the range of data available in our measured spectrum. As can be seen in table 5, little change of the g factor is expected due to this centrifugal force effect (less than 1%), far less change than the experimental error limits of our measurements. A relatively good numerical agreement between calculated g_{xx} and g_{zz} values and the appropriate experimental values was also achieved.

4. Discussion

For the molecules studied, the Zeeman splitting of the rovibrational levels in the magnetic field is too small to be directly measured using a medium-resolution experiment. Nevertheless, the perturbation of the molecular wavefunctions gives rise to a substantial MVCD signal that can be easily monitored with a medium-resolution spectrometer. The key issue in the analysis of the experimental spectra lies in the proper interpretation of the MVCD intensities in terms of the underlying Zeeman perturbation patterns (splittings and shifts). Unlike in the case of high-resolution experiments, where the energetic consequences of the Zeeman effect can be monitored directly, MVCD must determine these indirectly through intensity measurement. The advantage, of course, is enhanced sensitivity. For more complex spectra, a proper theoretical model is necessary for analysis and understanding of the experimental results. Previously {14, 15}, we adopted Stephens' two-state theory of MCD to apply

to the MVCD of simple molecules using moment analyses of the spectra. However, this approach is dependent on assuming that there is an insignificant vibrational contribution to the molecular g value which is not strictly true, in general.

4.1. Diatomic calibration analyses and simulation

In our experimental MVCD spectra for diatomics, only symmetrical derivative-shaped peaks are observed which is consistent with the fact that only A terms are detected and only A terms are expected. B terms (due to coupling between states as caused by the magnetic field) have only minor contributions to the MVCD spectra seen with rotational resolution. In the condensed phase where rotations are quenched and, consequently, A term contributions are generally reduced, this is not always the case {1–4}. C term contributions, which arise from differences in the populations of the ground state components which are split in energy by the magnetic field, are also very small in this case {14, 26}. The energy splittings induced by the magnetic field are negligible if compared to kT. The splitting between M states at 8 Tesla for $g = 0{\cdot}3$ (in nuclear magneton units) is only $0{\cdot}000\,61\ \mathrm{cm}^{-1}$ while $kT \approx 200\ \mathrm{cm}^{-1}$ at room temperature.

The simulated spectra for well studied diatomic molecules, such as $D^{35}Cl$, do agree well with the experimental results. This agreement between the simulated and experimental spectra further calibrates the MVCD technique and verifies the validity of the use of moment analysis for MVCD spectral analysis in situations where the g-value is relatively independent of J'' and v, the rotational and vibrational quantum numbers of ground and excited states. Thus MVCD is demonstrated to be a viable alternative technique for study of the molecular Zeeman effect in well resolved rotational transitions.

For most previous analyses of MVCD spectra, a major assumption has been made that $g_{v=1}$ is equal to $g_{v=0}$. Since this assumption has already been clearly demonstrated to be inapplicable for interpretations of the methane (CH_4 and CD_4) and haloform MVCD {40–43}, the effect on the MVCD of varying the $g_{v=1}/g_{v=0}$ ratio for $D^{35}Cl$ has been simulated as illustrated in figure 2. As noted above, the spectrum calculated for $g_{v=1} = g_{v=0}$ yields the best simulation of the experimental A_1/D_0 ratios derived from the RR MVCD and absorption spectra. Use of this A_1/D_0 criteria accounts for the fact that the R branch intensity of the simulated absorption spectrum is slightly higher than the P branch intensity while the P and R branch intensities appear to be roughly the same in the experimental absorption spectrum (see figure 1). This discrepancy is due to an error in the experimental determination of the relative dipolar intensity distribution only which is, at least in part, an experimental difficulty in photometric accuracy at the limiting resolution of the spectrometer. The consistency of our computed A_1/D_0 values for simulation and experiment confirms that the simulation contains a correct representation of the magnetic effect and that it reproduces the observed experimental Zeeman effect as represented by A_1/D_0. This means that, within our experimental error {14, 15}, the assumption that $g_{v=1}$ is the same as $g_{v=0}$ is valid for $D^{35}Cl$ and that this is also valid for CO and $H^{35}Cl$ as well, since the same pattern holds {14, 15}.

The results in figure 5 being statistically equivalent to a zero slope line for a plot of g_e vs J'' indicate that the simulation result using $g_{v=1} = g_{v=0}$ agrees with the experimental results. In addition, SCF level calculations of the molecular g values at different molecular bond lengths of HCl have shown that while the rotational g-value

should change from the $v = 0$ to $v = 1$ state {15}, this effect would be too small to observe using MVCD. Thus the assumption of constant g-value made in the analyses of experimental MVCD spectra is justified within our experimental constraints and yields valid molecular Zeeman results in these cases of diamagnetic diatomic molecules for which we have applied the above approximations.

4.2. Symmetric top, NH_3, simulation

The agreement between the simulated and experimental spectra of ammonia are qualitatively satisfactory. The correct sign pattern, general intensity pattern, and, for low J values, the magnitude of the g values are found. However, the simple assumption of a constant g value that is built into interpreting the results of the moment analysis method, is not justified in this case where the ground and excited state g values are significantly different, as documented in table 2. In the R branches (a and s) of the ν_2 rovibrational band, which have better developed MVCD structure, a clear increase in effective g value with increase in J″ is evident from the analyses of the experimental data. However, the quantitative aspects of this trend are not large enough to provide a reliable measure of the difference in g value. This definitely is a S/N problem that in principle could be solved by more extensive co-addition of spectra and consequent signal averaging over a longer time period. We have found that increasing the pressure to increase signal size is not a reasonable solution to this problem, since photometric inaccuracies in our instrument then become greater. Perhaps use of an alternate interferometer design might help in this regard.

The simulated NH_3 effective g values for the ν_2 transitions also increase with J″ in the R branch. Thus the experimental data are in agreement with the qualitative observation that $g_{v=1}$ is larger than $g_{v=0}$, which is consistent with the experimentally derived values in the literature {31, 44}. As seen in the simulated results in tables 3 and 4, the differential in g value should lead to a $< 5\%$ variation for sP and sR branches and somewhat more for the K-resolved aP and aR branches. Even a 10% change appears to be difficult to identify in these data due to fluctuations in the moments arising from random noise (primarily from the detector). We must suggest that this S/N limitation may not be acting alone for these 0·1 cm^{-1} MVCD results. The experimental MVCD g values determined here are all systematically high compared to the simulated values. In this regard, it is interesting to note that in our 0·5 cm^{-1} resolution MVCD study of NH_3, the g values tended to be smaller {16}. This does suggest some difficulty of the spectrometer in attaining the full photometric accuracy needed for such precision intensity measurements. Such difficulties are well-known in the IR intensity community {45}. Here it is important to note that the g value determinations for low J″ transitions are in good agreement with the accepted values for the NH_3 g value determination ($g_{v=0}$) but S/N and perhaps some other instrumental limitation at high J″ values prevent reliable determination of Δg and consequently of $g_{v=1}$ (which in this case is known to differ from $g_{v=0}$) {31, 44}.

Assuming that the published $v = 1$ g values are correct for NH_3, our MVCD determination of Δg must be viewed as qualitatively consistent with the known values. We have pursued, without finding a satisfactory conclusion, a series of computational experiments to determine what aspect of MVCD analysis leads to difficulty with $v = 1$ g values (or more precisely the Δg value) determination while the ground state ($v = 0$) g values are determined quite reliably. To offer a parallel analysis with the simulations for $D^{35}Cl$ (see figure 2), several MVCD spectra for NH_3 using different g-values for the

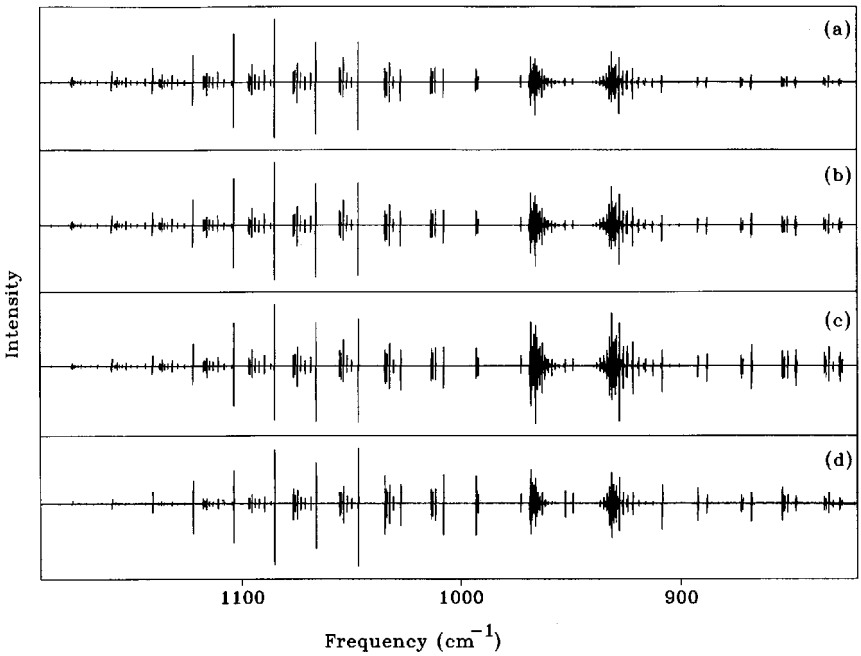

Figure 6. The simulated RR MVCD spectrum of NH_3 at 1 tesla with: (a) the g values in the $v = 1$ vibrational state being 10% higher than those listed in table 2; (b) the g values in the $v = 1$ vibrational state being the same as those listed in table 2; (c) the g values in the $v = 1$ vibrational state being 10% lower than those listed in table 2; and (d) the experimental MVCD spectra normalized to 1 tesla.

$v = 1$ state have also been simulated and are shown in figure 6. By reference to the experimental MVCD spectra for NH_3, (figure 6(d)), we can see that the simulated spectrum having g values for $v = 1$ that are 10% higher than the published values, deviates significantly from the experimental MVCD spectrum in a way that the P branch in figure 6(a) has much lower intensity than the R branch. By comparison, the experimental spectra appear to lie between the spectra simulated using the published $v = 1$ g values (figure 6(b)) and $v = 1$ g values which are 10% lower than the published values (figure 6(c)). When the simulated and the experimental absorption spectra for NH_3 are compared (figure 3), there is a larger difference between the dipole strength of the P and R branches for the simulated spectrum than for the experimental spectrum. So, if one normalizes the MVCD spectra in figure 6 by their corresponding absorbance spectra, i.e. determines A_1/D_0, the MVCD spectra simulated using the published $v = 1$ g values have the best agreement with the experimental MVCD spectrum.

From the above results, it is shown that MVCD could sense Δg values which are at least 10% of the ground state g value. However, for NH_3, because of the large random error in our intensity measurements, we are not able to extract the Δg value with reasonable accuracy from its more complex J and K dependent g_e values.

Finally, in this simulation of the ammonia MVCD spectrum, only the first order rotational Zeeman effect was taken into account. While this led to a satisfactorily simulation of the observed bandshape, the experimental transitions probably also include higher order Zeeman effects and perturbations from other states.

5. Conclusion

MVCD spectra of some diamagnetic, diatomic and symmetric top molecules have been simulated. Very good qualitative agreement has been obtained between the simulated and experimental spectra. Our work demonstrates that MVCD can give useful qualitative and reasonably accurate quantitative information about the interaction between small molecules and an external magnetic field.

The assumption used in the typical moment analysis of experimental MVCD that the rotational g value in the ground vibrational state is equal to that in the first excited vibrational state, is justified within our measurement accuracy for the diamagnetic diatomic molecules we have studied. Moreover, the effect of varying the rotational g values in the first excited vibrational state has been demonstrated theoretically by the analysis of simulated spectra of $D^{35}Cl$, and the experimental data have been shown to be consistent with $g_{v=0} = g_{v=1}$ for the diatomics studied. The MVCD spectra of these diatomic molecules serve as a calibration for using the MVCD technique to determine the molecular Zeeman effect.

The MVCD for NH_3 involves a more complex simulation. The detailed intensity pattern with increasing J'' value is qualitatively consistent with the simulation based on earlier measured g values for NH_3. The experimental NH_3 spectrum cannot be analysed quantitatively to the accuracy found with diatomic spectra due to the larger relative random error in both the 0·1 cm^{-1} resolution absorption and MVCD intensity measurements used. Comparison of simulations with varying g values showed that the published results gave the best fit. That MVCD can detect a difference in excited state and ground state g value has been demonstrated in our work on methane {40} and the haloforms {41, 42} and more recently for acetylene {38}. This work demonstrates that simulation plus A_1/D_0 determination provides a means of analysis of MVCD spectra in terms of specific excited and ground state g values.

This work was partially supported by a grant from the National Science Foundation (CHE 85 11753) and a Senior Scholar (T.A.K.) and Dean's Scholar (C.N.T.) awards from the University of Illinois. C.N.T. would also like to thank Mrs Philip L. Hawley for the Philip L. Hawley Fellowship administered through the University of Illinois at Chicago. We would like to thank Dr Lou Pierce for the program 'Contour' used to calibrate our own intensity simulation and Professor Donald Levy for help in its implementation.

Appendix A

Rotationally resolved MVCD

The general theory of MCD was elaborated by Stephens {26} for the case of molecules in the condensed phase. For circular dichroism spectra, the difference in absorption for left and right circularly polarized light is measured. When corrected for path length the differential extinction can be related to theoretical quantities as:

$$\Delta\varepsilon = \varepsilon_L - \varepsilon_R = 2\omega N_A \frac{n_2^L - n_2^R}{2{\cdot}303cN} \qquad (A\,1)$$

where N is number of molecules per volume, N_A is the Avogadro number, c is the

velocity of light, n_2^L and n_2^R is the imaginary part of the refractive index for left and right circular polarized light, respectively. Stephen's result for MCD can be re-written for a rotation–vibrational transition $|J''K''M''\rangle \rightarrow |J'K'M'\rangle$ as

$$\Delta\varepsilon = \pi\omega N_A \frac{|\langle J''K''M''|\mu_+|J'K'M'\rangle|^2 - |\langle J''K''M''|\mu_-|J'K'M'\rangle|^2}{2{\cdot}303c\varepsilon_0\bar{h}} \tag{A 2}$$

where ω is the frequency of the transition, ε_0 is the vacuum permitivity, and $\bar{h}$ is Planck's constant. The expression of the electric dipole matrix elements as spherical tensor elements is very convenient for the description of rotationally resolved MVCD. Here the convention is used whereby the space fixed Z axis is taken to be collinear with the magnetic field direction which is also collinear with the direction of light propagation. The dipole operators can be transformed to a spherical tensor operator notation as:

$$\begin{aligned} T(1,\pm1) &= \mp(\mu_X \pm i\mu_Y)/\sqrt{2} = \mp\mu_\pm \\ T(1,0) &= \mu_Z. \end{aligned} \tag{A 3}$$

The tensor matrix elements can be directly evaluated in the basis of rotational eigenfunctions of the angular momentum operator, using the Wigner–Eckart theorem. Thus for diatomic or symmetric top molecules:

$$\begin{aligned} \langle v', J'K'M'|\mu_\pm|v'', J''K''M''\rangle &= \mp\langle v', J'K'M'|T(1,\pm1)|v'', J''K''M''\rangle \\ &= \mp\langle 1\pm1 J''M''|J'M'\rangle\langle v', J'K'\|T\|v'', J''K''\rangle \end{aligned} \tag{A 4}$$

where the reduced matrix element $\langle v', J'K'\|T\|v'', J''K''\rangle$ is independent of the molecular space orientation, and $\langle 1\pm1 J''M''|J'M'\rangle$ is the Clebsch–Gordan coefficient, which can be evaluated analytically. Obviously, $K'' = K' = 0$ for diatomic molecules.

Appendix B

Moment analysis of RR MVCD spectra

Here we will investigate the validity of moment analysis of MVCD spectra for the case of rovibrational transitions. Let the ground state be determined by the wavefunction $|v''J''K''M''\rangle$ with the energy $\varepsilon = -g_{v''}\mu_N M''\mathscr{B}_z$, while the excited state can be written as $|v'J'K'M'\rangle$ with energy $\varepsilon = \varepsilon_0 - g_{v'}\mu_N M'\mathscr{B}_z$, and transitions are allowed for $M' = M''\pm1$. In these relationships, $g_{v''}$, $g_{v'}$ denote the ground and excited state g values, and they are dependent generally on J and K; μ_N is the nuclear magneton; and $\mathscr{B}_z$ is the intensity of the magnetic field. The g values for the ground and excited vibrational states generally differ by

$$\Delta g = g_{v'} - g_{v''}. \tag{B 1}$$

Because of the small magnitude of the rotational level splitting caused by the magnetic field for diamagnetic molecules, experimentally only the transition $J''\rightarrow J'$ for diatomics and $J''K''\rightarrow J'K'$ for symmetric top molecules will be seen, averaged over the M quantum numbers. We are interested in the result of the previously described moment analyses of the MVCD and absorption bands. Let us denote the 'experimental' or effective g-value, g_e, according to equations (7) and (8). The absorption

and the MVCD signal is given by equation (6). Combining equations (7), (8) and (6), we obtain the following expression for the observable g factor:

$$g_e = g_V + \Delta g \frac{\sum_{M''} \langle J' - M'' - 1 J'' M'' | 1 - 1 \rangle^2 M'' - \sum_{M''} \langle J' - M'' + 1 J'' M'' | 11 \rangle^2 M''}{2 \sum_{M''} \langle J' - M'' - 1 J'' M'' | 1 - 1 \rangle^2}. \quad (B2)$$

After evaluation of the Clebsch–Gordan coefficients and summation over all allowed M'', we get the expressions in equation (9).

If a moment analysis is applied for a band with unresolved K components, an effective g value averaged over $J''+1$ K transitions would be observed.

References

{1} KEIDERLING, T. A., 1981, J. chem. Phys., **75**, 3659.
{2} DEVINE, T. R., and KEIDERLING, T. A., 1983, J. chem. Phys., **79**, 5796.
{3} DEVINE, T. R., and KEIDERLING, T. A., 1987, Spectrachim. Acta, **43A**, 627.
{4} DEVINE, T. R., and KEIDERLING, T. A., 1986, Chem. Phys. Lett., **124**, 341.
{5} DEVINE, T. R., 1984, Ph. D. Thesis, University of Illinois at Chicago.
{6} DEVINE, T. R., and KEIDERLING, T. A., 1984, J. phys. Chem., **88**, 390.
{7} DEVINE, T. R., and KEIDERLING, T. A., 1985, J. chem. Phys., **83**, 3749.
{8} DEVINE, T. R., and KEIDERLING, T. A., 1987, J. chem. Phys., **87**, 5051.
{9} CROATTO, P. V., and KEIDERLING, T. A., 1988, Chem. Phys. Lett., **144**, 455.
{10} CROATTO, P. V., 1990, Ph. D. Thesis, University of Illinois at Chicago.
{11} PAWLIKOWSKI, M., and KEIDERLING, T. A., 1984, J. chem. Phys., **81**, 4765.
{12} PAWLIKOWSKI, M., and DEVINE, T. R., 1985, J. chem. Phys., **83**, 950.
{13} PAWLIKOWSKI, M., 1986, Chem. phys. Lett., **128**, 172.
{14} WANG, B., and KEIDERLING, T. A., 1993, J. chem. Phys., **98**, 903.
{15} TAM, C. N., and KEIDERLING, T. A., 1993, J. molec. Spectrosc., **157**, 391.
{16} WANG, B., YOO, R. K., CROATTO, P. V., and KEIDERLING, T. A., 1992, J. phys. Chem., **96**, 2422.
{17} WANG, B., YOO, R. K., CROATTO, P. V., and KEIDERLING, T. A., 1991, Chem. Phys. Lett., **180**, 339.
{18} ROSENBLUM, B., NETHERCOT, A. H., and TOWNES, C. H., 1958, Phys. Rev., **109**, 400.
{19} OZIER, I., YI, P. N., KHOSLA, A., and RAMSEY, N., 1967, J. chem. Phys., **46**, 1530.
{20} CRAPO, L. M., and RAMSEY, N., 1968, J. chem. Phys., **49**, 2314.
{21} KAISER, E. W., 1970, J. chem. Phys., **53**, 1686.
{22} DE LEEUW, F. H., and DYMANUS, A., 1971, Symp. Molec. Spectrosc., Columbus, Ohio, Paper R10.
{23} HERZBERG, G., 1945, Molecular Spectra and Molecular Structure, Vol. II, (Toronto: Van Nostrand).
{24} GORDY, W., and COOK, R. L., 1984, Microwave Molecular Spectra, third edn, (New York: Wiley).
{25} HÜTTNER, W., 1982, Landolt±Börnstein Numerical Data and Functional Relationships in Science and Technology, Vol. II/14, edited by K.-H. Hellwege, and A. M. Hellwege, (Berlin: Springer-Verlag).
{26} STEPHENS, P. J., 1976, Adv. chem. Phys., **35**, 197.
{27} ZARE, R. N., 1988, Angular Momentum (New York: Wiley).
{28} HERMAN, R., and WALLIS, R. F., 1955, J. chem. Phys., **23**, 637.
{29} SPECTRA CALC, 1988, Galactic Industries Corporation, Nashua, NH.
{30} PIERCE, L., 1993, Contour—spectra simulation program, University of Notre Dame.
{31} HÜTTNER, W., FRANK, U. E., MAJER, W., MAYOR, K., and SPIRKO, V., 1988, Molec. Phys., **64**, 1233.
{32} PIEPHO, S. B., and SCHATZ, P. N., 1983, Group Theory in Spectroscopy and Applications to Magnetic Circular Dichroism (New York: Wiley).

{33} YOO, R. K., CROATTO, P. V., WANG, B., and KEIDERLING, T. A., 1990, Appl. Spectrosc., **45**, 231.
{34} WANG, B., and KEIDERLING, T. A., 1995, Appl. Spectrosc., **49**, 1347.
{35} KEIDERLING, T. A., 1990, Practical Fourier Transform Infrared Spectroscopy, edited by J. R. Ferraro, and K. Krishana, (San Diego: Academic).
{36} TAM, C. N., 1995, Ph. D. Thesis, University of Illinois at Chicago.
{37} TAM, C. N., and KEIDERLING, T. A., 1995, Chem. phys. Lett., **243**, 55.
{38} TAM, C. N., BOUR, P., and KEIDERLING, T. A., 1996, J. chem. Phys., in press.
{39} AMOS, R. D., 1984–1990, CADPAC version 5.0, SERC Laboratory, Daresbury, UK.
{40} WANG, B., and KEIDERLING, T. A., 1994, J. phys. Chem., **98**, 3957.
{41} WANG, B., TAM, C. N., and KEIDERLING, T. A., 1993, Phys. Rev. Lett., **71**, 979.
{42} WANG, B., and KEIDERLING, T. A., 1994, J. chem. Phys., **101**, 905.
{43} WANG, B., 1993, Ph. D. Thesis, University of Illinois at Chicago.
{44} HÜTTNER, W., FRANK, U. E., and NOWICKI, P., 1992, Chem. phys. Lett., **196**, 614.
{45} PERSON, W., and STEELE, D., 1974, Molecular Spectroscopy, Vol. 2, edited by R. F. Barrow, D. A. Long, and D. J. Millen, (London: The Chemical Society).